Aerosol Science and Technology, 39:249–260, 2005

ISSN: 0278-6826 print / 1521-7388 online
DOI: 10.1080/027868290925958

Measurement of Wavelength-Resolved Light Absorption by Aerosols Utilizing a UV-VIS Extinction Cell

M. Schnaiter,[1] O. Schmid,[2] A. Petzold,[3] L. Fritzsche,[3] K. F. Klein,[4] M. O. Andreae,[2] G. Helas,[2] A. Thielmann,[2] M. Gimmler,[1] O. Möhler,[1] C. Linke,[1] and U. Schurath[1]

[1] *Forschungszentrum Karlsruhe, Institute of Meteorology and Climate Research, Karlsruhe, Germany*
[2] *Max Planck Institute for Chemistry, Department of Biogeochemistry, Mainz, Germany*
[3] *German Aerospace Center (DLR) Oberpfaffenhofen, Institute of Atmospheric Physics, Wessling, Germany*
[4] *University of Applied Sciences Giessen-Friedberg, Department of Information Technology, Friedberg, Germany*

The principle, technical details, and performance of the long path extinction spectrometer (LOPES), a new folded-path extinction cell with a spectral range from the mid-UV (200 nm) to the near infrared (1015 nm), is presented. Using nonabsorbing glass beads the measured extinction spectrum of LOPES was validated by Mie calculations and was compared with scattering coefficients in the visible measured by a three-color integrating nephelometer (TSI, mod. 3563). For absorbing aerosols (here soot and biomass burning aerosol with single-scattering albedos of about 0.2 and 0.74 at 550 nm), LOPES was combined with a TSI 3563 nephelometer to determine the wavelength-dependent absorption coefficients from the difference of the extinction and scattering coefficients. These absorption coefficients were found to agree with the measurements by two state-of-the-art absorption techniques, the multiangle absorption photometry (MAAP) and photoacoustic spectrometry (PAS), which measure the absorption coefficient at the single wavelength of 532 nm and 670 nm, respectively. Finally, based on a comprehensive analysis of the TSI 3563 nephelometer errors and their propagation into the determination of the absorption coefficients from the LOPES and nephelometer data, we discuss implications for improving in situ measurements of the optical properties of atmospheric aerosols.

Received 3 August 2004; accepted 13 January 2005.
We thank Elisabeth Kranz for filter sampling and accomplishment of the thermographic carbon analysis. Georg Scheurig is thanked for providing SEM micrographs. This research was funded by the Max Planck Society and the Helmholtz Association of National Research Centres.
Address correspondence to M. Schnaiter, Forschungszentrum Karlsruhe, Institute of Meteorology and Climate Research, Karlsruhe, Germany. E-mail: martin.schnaiter@imk.fzk.de

INTRODUCTION

Atmospheric aerosols have a direct and indirect impact on the radiative balance of the atmosphere, and therefore they may significantly affect the regional and global climate (Houghton et al. 2001). The direct impact of aerosols on the short-wave solar flux through the atmosphere depends on the aerosol optical depth, the single-scattering albedo (SSA), the phase function (in particular the asymmetry factor), and the wavelength dependence of these quantities (Chylek and Wong 1995). Although recent field experiments such as LACE (Petzold et al. 2002), SCAR-B (Kaufman et al. 1998), TARFOX (Russell et al. 1999), INDOEX (Ramanathan et al. 2001), and SAFARI 2000 (Eck et al. 2003) have substantially enhanced the available information on optical properties of atmospheric aerosol.

Historically, in situ measurements of the aerosol single-scattering albedo, defined as the relative contribution of scattering to extinction (where extinction is scattering plus absorption), were mostly performed with integrating nephelometers (scattering) and filter-based absorption techniques such as the particle soot absorption photometer (PSAP) or the Aethalometer. While all of these methods suffer from potentially significant systematic uncertainties (Anderson et al. 1996; Bond et al. 1999; Weingartner et al. 2003), the uncertainties in nephelometers are reasonably well understood and correctable based on Mie calculations (Heintzenberg and Charlson 1996; Anderson et al. 1996). On the other hand, filter-based absorption techniques suffer from biases due to filter substrate and cross-sensitivity to aerosol light scattering, which are acknowledged but not well understood (Bond et al. 1999; Weingartner et al. 2003). Therefore, these aerosol absorption techniques have frequently been calibrated in the laboratory based on the measured difference of extinction and scattering utilizing optical

extinction cells and nephelometers, respectively (Reid et al. 1998; Bond et al. 1999; Weingartner et al. 2003; Sheridan et al. 2005). However, since the calibration parameters may depend on the type of aerosol sampled, more reliable absorption techniques have been developed recently, such as photoacoustic spectrometry (Arnott et al. 2000) and the multiangle absorption photometry (MAAP; Petzold et al. 2005).

In this study we discuss the principle, technical details, and performance of a novel extinction cell, the long path extinction spectrometer (LOPES), which is the first folded-path optical extinction cell with a spectral range from the mid-UV (200 nm) to the near infrared (1015 nm). Extending the spectral range to the mid-UV is expected to provide valuable information about the electronic structure of carbonaceous aerosols (Schnaiter et al. 2003). The applicability of the LOPES to aerosol optical studies over its entire spectral range is first investigated with purely scattering aerosol (here quartz glass beads), for which an integrating three-wavelengths nephelometer combined with Mie calculations serves as reference. For absorbing aerosol (carbonaceous particles from spark discharge, a diesel engine, and biomass burning), the difference between extinction (LOPES) and scattering (nephelometer) was compared to two state-of-the-art absorption techniques, the photoacoustic spectrometer (PAS; Arnott et al. 2000) and the MAAP (Petzold et al. 2005), which measure absorption at a wavelength of 532 and 670 nm, respectively. Finally, based on an error analysis of the LOPES we discuss implications for improving the in situ determination of optical properties of atmospheric aerosol are discussed.

OPTICAL TECHNIQUES

In this section we discuss the principle and technical details of the optical instruments used here, where the focus is on LOPES. While the PAS and MAAP are also described in some detail, we refer to Heintzenberg and Charlson (1996) and Anderson et al. (1996) for details on integrating nephelometers.

The New Extinction Spectrometer LOPES

Theoretical Background

The extinction of light passing through an aerosol layer is described by Bouguer-Lambert's law

$$\ln\left\{\frac{I_0}{I}\right\} = \tau, \qquad [1]$$

where I_0 and I are the incoming and transmitted light intensities, and τ is the optical depth of the aerosol layer. Since $\tau = b_{\text{ext}} \cdot L$, where b_{ext} and L is the extinction coefficient and the optical path length within the aerosol layer, optical extinction cells determine b_{ext} from

$$b_{\text{ext}} = \frac{\ln\left(I_0/I\right)}{L}. \qquad [2]$$

For an aerosol ensemble with uniform refractive index, the extinction coefficient at a specific wavelength λ is given by

$$b_{\text{ext}}(\lambda) = \int C_{\text{ext}}(m(\lambda), D_p, \lambda) \cdot N(\ln D_p) \cdot \mathrm{d}\ln D_p, \qquad [3]$$

where C_{ext} is the extinction cross section of a particle with diameter D_p and refractive index $m(\lambda)$ at the wavelength λ, and $N(\ln D_p)$ is the number size distribution. If in addition to the extinction coefficient the scattering coefficient b_{sca} is known, the absorption coefficient b_{abs} can be calculated from

$$b_{\text{abs}} = b_{\text{ext}} - b_{\text{sca}}. \qquad [4]$$

Extinction of light can be interpreted as the interference of an incident plane wave with the spherical wavelets scattered by the particles *exactly* in the forward direction (Bohren and Huffman 1983). Since, in practice, any measurement of I_0 and I covers a finite acceptance angle θ_{acc}, the measured intensity in forward direction ($\theta = 0$) is systematically enhanced by the fraction of light scattered in near-forward direction ($0 < \theta \leq \theta_{\text{acc}}$). For optical extinction cells, this enhances the measured intensity I and consequently reduces the measured extinction (see Equation [2]). The magnitude of this bias increases with θ_{acc} and size parameters $x = \pi \mathrm{D_p}/\lambda \gg 1$. Using scalar diffraction theory (Bohren and Huffman 1983; Moosmüller and Arnott 2003) and assuming nonabsorbing aerosol (SSA = 1), we can estimate the error in b_{ext} and account for it, if necessary. As seen from Figure 1, the error introduced by the finite acceptance angle θ_{acc} is <1%, if $x \sin(\theta_{\text{acc}})$ <0.28.

Instrument Setup

The LOPES (Figure 2) is an improved version of the single-pass flow tube extinction spectrometer described by Schnaiter et al. (2003). Notable changes are a doubling of the optical path length to improve the sensitivity and reduce the extinction

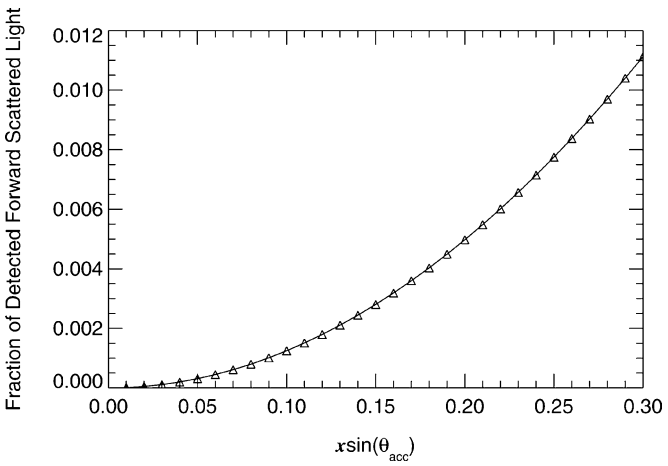

FIG. 1. Fractional error in the measured extinction coefficient of an aerosol with size parameter $x = \pi D_p/\lambda$ due to a finite acceptance angle θ_{acc}.

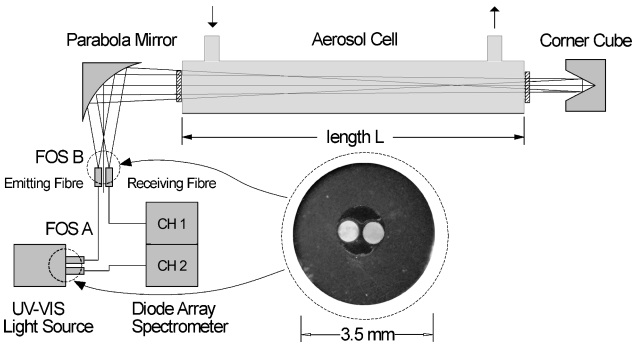

FIG. 2. Schematics of the LOPES system. The magnified image of the fiber connector jacket shows the side-by-side alignment of the emitting and receiving fibers.

error, and an extension of the spectral range to ∼200 nm by using UV-solarization stabilized fiber optics. Currently, two LOPES systems exist with flow tube lengths of 3.5 and 5.0 m and inner diameters of 26 and 44 mm, respectively. As shown in Figure 2 the optical length is twice the geometric length, L, of the flow tube due to optical path folding with a hollow corner cube mounted at the far end of the tube (26 mm tube: Melles Griot, mod. 99302CCH0011; 44 mm tube: Linos, mod. 033959, both with UV-enhanced aluminium coatings). The light from a deuterium/halogen lamp combination emitting from 190 to 1500 nm (Avantes, mod. DH-2000-FHS-DUV) is connected to the flow tube via fiber optics as described below. Spectral analysis of the light source and of the light transmitted through the tube is performed by a two-channel UV-VIS diode array spectrometer (Zeiss, mod. MCS 55, spectral resolution 2.5 nm). Two spectrometers are operated interchangeably at the LOPES systems with dynamic ranges of 15 and 16 bit and with multiplexed and separated channel readout, respectively.

Two hydrogen-doped, UV-stabilized UVMI-fibers with core diameters of 400 μm are mounted sidebyside on a xyz-translation stage in front of a 90° off-axis parabola mirror (Coherent, mod. 43-8945 with UV-enhanced aluminium coating) with an off-axis focal length of $f = 101.6$ mm. The design and performance of the fiber optical system is described in the next section. Since the emitting fiber has a finite diameter, the positioning of the fiber end in exactly the focal plane of the mirror would result in a divergent beam with a divergence angle of 2 mrad. This divergence would be far too large to realize optical path lengths of several meters within the narrow LOPES flow tubes. Therefore, it is advantageous to position the fibers at an object distance that results in a magnification of 33 and 48 of their end faces at the far end of the 3.5 and 5.0 m tubes, respectively. Since the corner cube offsets the reflected beam symmetrically to the optical axis, the image of the emitting fiber is refocused on the receiving fiber. The optical system can be aligned easily by moving the two fibers into a position symmetric to the optical axis. This results in an acceptance angle θ_{acc} of about 4 mrad for both LOPES instruments, which limits the diameter to $D_p < 4.5$ μm, if the acceptance error is to be limited to less than 1% in b_{ext} over the whole spectral region covered by LOPES (see Figure 1).

In practice the accuracy of extinction measurements with LOPES mainly depends on the stability of the optical alignment. To minimize experimental errors due to mechanical stress and vibrations the coupling optics, the flow tube, and the corner cube are mounted on an optical bench (LINOS, aluminium profile system X95). A critical issue is the fixation of the optical fibers in front of the parabola mirror, since it controls the quality of the coupling between the optical cell, the light source, and the spectrometer. This part of the optics was found to be very sensitive to temperature fluctuations of the order of a few degrees. In order to mitigate temperature fluctuations the coupling optics were encapsulated in a thermally insulating box. For long-term measurements without periodical recordings of particle-free air spectra to correct for temperature-induced baseline drifts it is necessary to stabilize the temperature inside the insulating box actively. During the experiments reported in this article, particle-free air spectra were recorded every 10 minutes. Thus the accuracy, which is defined by instabilities of the baseline, was in the range of the instrument noise of 20 Mm^{-1} and 40 Mm^{-1} determined for the 10 and 7 m LOPES systems, respectively.

Design of the Fiber Optical System

The fiber optical system (FOS) is composed of four solarization-stabilized UVMI fibers with 400 μm core diameter. The FOS contains two fiber combinations (FOS A and FOS B), each one composed of two fibers, which are at one end aligned sidebyside in a standard SMA fiber connector jacket (Figure 2). This connector is connected for FOS A with the light source and for FOS B with the xyz-translation stage. FOS A and B are interconnected and connected to channel 1 and channel 2 of the UV-VIS spectrometer. Channel 1 analyses the light transmitted through the optical cell and channel 2 records the emission of the light source to correct for potential drifts in lamp emission.

Use of hydrogen-doped UVMI fibers avoids strong transmission losses in the $\lambda < 230$ nm spectral region due to the UV-C induced formation of color centers (E-centers) in the fiber material (Klein et al. 1997; Huebner et al. 2000). Since the defect formation in UVMI-fibers is balanced by hydrogen diffusion to and healing of the E-centers, the fiber transmission in the $\lambda < 230$ nm spectral region is time and temperature dependent. The time dependence of UV light transmission at 214 nm was characterized for the LOPES FOS at various temperatures down to −75°C. Figure 3 shows that down to a temperature of about −50°C a steady-state transmission level >70% is established within a few hours (inset in Figure 3). At room temperature the transmission in the $\lambda < 230$ nm range is almost unaffected by illumination with UV-C light and stabilizes within half an hour, resulting in a transmission reduction of less than 2%, using a total fiber length (emitting and receiving fiber) of 6 m. For two cases (20°C and −35°C) we have also shown the recovery of the fiber (increasing transmission) under dark conditions.

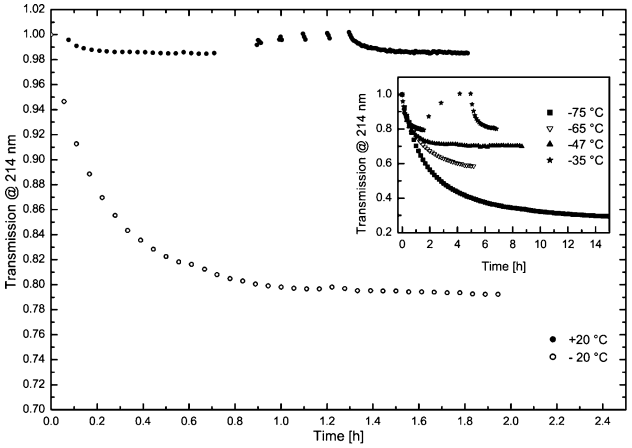

FIG. 3. Temperature dependence of UV light transmission through the fiber optical system composed of solarization stabilized hydrogen doped silica fibers. The curves show the fiber stabilization during UV light transmission as well as their recovering during dark phases.

Multiangle Absorption Photometry (MAAP)

Multiangle absorption photometry is based on simultaneous measurements of radiation transmitted through and scattered back from a particle-loaded fiber filter. A detailed description of the method is given by Petzold, Kramer, and Schönlinner (2002) and Petzold and Schönlinner (2004). In summary, an investigation of the angular distribution of light backscattered from and transmitted through a fiber filter has shown that the transmitted radiation is completely diffuse, while the backscattered radiation contains a diffusely scattered component and a Gaussian-distributed component that is connected to radiation "reflected" from a rough surface. The partitioning of backscattered radiation between diffuse and Gaussian types depends on the sampled aerosol. Hence, the data obtained from radiation measurements at several detection angles permits the full determination of the radiation fields in the forward and back hemispheres relative to the illuminating light source. The exact position of the detection angles was chosen such that the partitioning between diffuse and Gaussian types can be determined with highest resolution.

The determination of the aerosol absorption coefficient of the deposited aerosol uses radiative transfer techniques. The particle-loaded filter is treated as a two-layer system: the aerosol-loaded layer of the filter and the particle-free filter matrix. Radiative processes inside the layer of deposited aerosol and between this layer and the particle-free filter matrix are taken into account separately. The treatment of radiative processes that are relevant in such a two-layer system has to consider the layer optical properties T (fraction of transmitted radiation), F (fraction of forward-scattered radiation), B (fraction of backscattered radiation), and P (fraction of radiation passed through the particle-loaded filter) with $P = T + F$. The optical properties of the particle-free filter matrix (subscript M), the aerosol-loaded filter layer (subscript L), and the entire filter composed of the aerosol-loaded filter layer and the particle-free filter matrix (subscript F) have to be included. Diffuse (superscript*) and collimated (no superscript) incident radiation have to be distinguished.

The consideration of multiple scattering effects between the particle-loaded filter layer and the particle-free filter matrix, as well as scattering processes inside the aerosol layer, yield the following budget equations for the ratio of radiation passed through a particle-loaded and a blank filter, $P_F/P_F{}^{(0)}$, and for the ratio of radiation scattered from a particle-loaded and a blank filter, $B_F/B_F{}^{(0)}$, (Petzold and Schönlinner 2004):

$$\frac{P_F}{P_F^{(0)}} = \frac{T_L + F_L}{1 - B_L^* B_M}, \qquad [5a]$$

$$\frac{B_F}{B_F^{(0)}} = P_L^* \frac{T_L + F_L}{1 - B_L^* B_M} + \frac{B_L}{B_M}. \qquad [5b]$$

The coupled Equations (5a) and (5b) are solved by calculating the required properties F_L, B_L, $P_L{}^*$, and $B_L{}^*$ via the variation of the independent variables $\mathrm{LOD} = \ln T_L$, which corresponds to the optical depth of the aerosol-loaded filter layer, and $\mathrm{SSA_L}$, the single-scattering albedo of the aerosol-loaded filter (Petzold and Schönlinner 2004). From the final values LOD and $\mathrm{SSA_L}$, the method-related absorption coefficient $b_{\mathrm{abs}}^{\mathrm{MAAP}}$ is calculated as

$$b_{\mathrm{abs}}^{\mathrm{MAAP}} = -\frac{A}{V} \cdot (1 - \mathrm{SSA_L}) \cdot \mathrm{LOD}. \qquad [6]$$

Intensive calibration and intercomparison studies using light-absorbing and light-scattering particles (Petzold et al. 2005) have proven that absorption coefficients measured by MAAP at $\lambda = 670$ nm are in close agreement with absorption coefficients measured by in situ methods like photoacosutic spectrometry and extinction plus scattering coefficient measurements. The approach of analyzing the optical properties of a particle-loaded filter by radiative transfer methods turned out to be a valuable method for adequately treating the impact of filter loading and scattering processes by particles and filter material on the measurement of the aerosol absorption coefficient. Furthermore, the method does not require any calibration for the measurement of the aerosol absorption coefficient (Petzold and Schönlinner 2004). The deviations between in situ measured absorption coefficients and values derived from MAAP measurements are less than 5%. The overall method uncertainty of $b_{\mathrm{abs}}^{\mathrm{MAAP}}$ is 12% as derived from an assessment of all important sources for measurement uncertainties (Petzold and Schönlinner 2004). The deviations between in situ measured and MAAP-derived absorption coefficients are thus within the uncertainty of the method.

Photoacoustic Spectrometry (PAS)

Photoacoustic spectrometers (PAS) determine aerosol light absorption by converting the absorbed energy into an acoustic wave, which is detected by a sensitive microphone (Terhune and Anderson 1977). In contrast to filter-based methods like the MAAP, PSAP, and Aethelometer, this measurement is performed on particles in their suspended state. Unlike filter-based methods, our measurements with purely scattering aerosol (ammonium sulfate) have shown that the PAS is a zero-based technique, i.e., it displays no response to aerosol light scattering.

In a PAS the sample aerosol is drawn through an acoustic resonator, which is illuminated by a power-modulated laser. The sample aerosol and carrier gas molecules periodically absorb laser energy, which is rapidly transferred as heat to the carrier gas, resulting in a standing acoustic wave in the acoustic resonator. A calibrated microphone measures the pressure amplitude P_m of this acoustic wave, which is directly related to the PAS absorption coefficient $b_{\text{abs}}^{\text{PAS}}$ according to Rosencwaig (1980),

$$b_{\text{abs}}^{\text{PAS}} = P_m \frac{\pi^2 A_{\text{res}} f_0}{P_L Q (\gamma - 1)}, \qquad [7]$$

where A_{res}, f_0, and Q are the cross-sectional area (here 2.18 cm^2), the acoustic resonance frequency (~1500 Hz), and the quality factor of the resonator (~75). P_L is the modulated average laser power and γ is the ratio of the isobaric and isochoric specific heats of the carrier gas ($\gamma_{\text{air}} = 1.4$).

The device used here is a refined version of the PAS described by Arnott et al. (1999). It incorporates a frequency-doubled ($\lambda = 532$ nm) diode laser-pumped Nd:YAG laser, which is power-modulated by a chopper. P_L (here ≈50 mW) is monitored by a photodiode mounted on an integrating sphere. To avoid systematic errors due to temperature and pressure drifts in $_0$ and Q, both parameters are continuously monitored and optimized for acoustic resonance utilizing a piezoelectric disc (Arnott et al. 1999).

The main sources for measurement uncertainties of the PAS are zero point instabilities and a cross-sensitivity to NO_2 (at 532 nm). Zero-point instabilities due to, e.g., inadvertent heating of the resonator walls by stray light are readily accounted for by repeated zero-point calibrations with particle-free air. Over the course of several hours we observed typical zero-point drifts of about 1.6 Mm^{-1}. For absorption measurements at 532 nm, there is a relatively weak cross-sensitivity to NO_2 (Arnott et al. 2000), which was accounted for by continuously monitoring gas-phase NO_2 with a chemiluminescence detector (CLD 780 TR, Eco Physics, Switzerland) described by Kley and McFarland (1980). Finally, the accuracy of the PAS depends on the uncertainties in P_m, A_{res}, f_0, P_L, and Q (see Equation [7]), and hence to a large degree on the accuracy of the microphone and photodiode calibrations. Combining all of these effects, the overall accuracy of the PAS is estimated as about 5.0% for the relatively large absorption coefficients reported here (>50 Mm^{-1}).

For quality assurance, the 5% accuracy was verified by a PAS self-test. For this test relatively high levels of NO_2 (here ~1000 ppm in synthetic air) were supplied to the PAS (Arnott et al. 2000), which resulted in a measurable attenuation of the laser intensity in the resonator. Using Equation (1) in the form $I = I_0 \exp(-b_{\text{abs}} L_{\text{res}})$, we have an alternative method to determine b_{abs}, where the optical length of the resonator L_{res} is 0.2486 m, and I and I_0, the laser intensities with and without NO_2 in the resonator, respectively, are determined by the photodiode of the PAS. We found that b_{abs} determined from Equations (7) and (1) agreed to within 2.3%, which confirms 5.0% as a conservative estimate of the PAS accuracy.

EXPERIMENTS AND RESULTS

As mentioned above, we performed experiments with three different types of laboratory- generated aerosols. First, nonabsorbing quartz glass beads (SSA = 1) of defined sizes were used to investigate the performance of LOPES over its entire wavelength regime utilizing a three-color integrating nephelometer (TSI, mod. 3563) and Mie calculations. Second, highly absorbing soot aerosol (here SSA ≈ 0.2 at 550 nm) and moderately absorbing biomass burning aerosol (here SSA ≈ 0.7 at 550 nm) was used in a closure study of extinction (LOPES), scattering (TSI 3563), and absorption coefficients (PAS, MAAP) to discuss the viability of determining wavelength-resolved absorption of atmospheric aerosols from the difference between extinction and scattering measurements.

Quartz Glass Beads

Two types of monodisperse quartz glass beads (Merck: Monospher® 500 and Monospher® 800) were dispersed with a rotating brush device (PALAS, mod. RBG 1000) in combination with a dispersion nozzle and fed into a large stainless steel reservoir container (3.7 m^3) from which both LOPES and the TSI 3563 nephelometer (450, 550, and 700 nm) sampled at flow rates of typically 5 liters per minute. Simultaneously, particle size distributions were measured with an aerodynamic particle sizer (APS; TSI, mod. 3321; 600 nm $< D_p <$ 10,000 nm) and a scanning mobility particle sizer (SMPS) consisting of a TSI 3071 DMA (20 nm $< D_p <$ 860 nm) and a TSI 3010 condensation particle counter (CPC).

The APS and SMPS measurements were fitted assuming lognormally distributed particle diameters. In case of the Monospher® 500 sample, a count median diameter (CMD) of 495 nm and a geometric standard deviation (σ_g) of 1.1 were deduced from the SMPS measurement in good agreement with the nominal diameter range given by the manufacturer (480 nm, 5% relative standard deviation). For the Monospher®800 particle sample, lognormal fits to the APS measurements resulted in a CMD and σ_g of 730 nm and 1.1, respectively, which is

also within the nominal diameter range given by the manufacturer (750 nm, 5% relative standard deviation). According to the discussion in the section "The new extinction spectrometer LOPES," these particles are small enough to avoid significant systematic lowering of the measured extinction coefficient due to near-forward scattered light. We used the bulk density of 1.9 g/cm^3 given by the manufacturer to convert the aerodynamic diameter measured by the APS to a Stokes diameter (i.e., the geometric diameter in case of spheres). Note that this density is significantly smaller than that of fused silica ($\sim$2.5 g/ cm^3).

Mie calculations were performed in the 200–1000 nm spectral range. We used the Mie code for concentrically coated spheres (Bohren and Huffman 1983), which has been extended to include the scattering phase function. All Mie calculations in this study assume uniform aerosol properties. Since the refractive index of the beads is not provided by the manufacturer, we used the value of n = 1.37 (λ = 589 nm) given by Bangs Laboratories Inc. (IN, USA) for quartz glass beads with the same bulk density (1.9 g/cm^3). This refractive index is significantly smaller than the corresponding value of fused silica (n = 1.46) consistent with the lower bulk density of the beads. Since a spectral refractive index for quartz beads is lacking in literature, we estimated its wavelength dependence by downscaling the well-known spectral refractive index of fused silica (Palik 1985) by 0.94 in order to match n = 1.37 of quartz beads at λ = 589 nm. Figure 4 compares the measured extinction spectra of the Monospher® 500 and Monospher® 800 beads with the results of Mie calculations. Best fits to the measured spectra were achieved for lognormal size distributions with median diameters of 520 and 780 nm, and narrow geometric standard deviations of 1.05 and 1.03, respectively. Good agreement is found between measured and calculated spectra, and especially the broad interference structure is well reproduced. However, discrepancies exist for the exact wavelength positions of the maxima and minima of the small scale "ripple structure" and for the near-infrared spectral slopes. Theoretical (Mishchenko et al. 1995) and experimental results by Schnaiter and Wurm (2002) have shown that these discrepancies can be explained by the presence of small agglomerates. Since these investigations also have shown that small aggregates do not completely flatten the sphere "ripples" in the extinction spectrum, the measured standard deviations ($\sim$1.1), which are slightly broader than those necessary to produce a "ripple structure" in the spectra (1.05 and 1.03), also indicates the presence of additional agglomerates.

Since the quartz beads have a nonabsorbing complex refractive index in the wavelength range from 200 to 1015 nm (Palik 1985), b_{ext} determined by LOPES should agree with the nephelometer measurements of b_{sca}, i.e., SSA should be equal to unity. The filled symbols in Figure 5 show the obtained single-scattering albedos, which are significantly smaller than unity at all three wavelengths of the TSI 3563 nephelometer (0.8 < SSA < 0.93). In Figure 5 the result of a further experiment with Monospher® 1200 aerosol (which was actually a mixture of Monospher® 1200 with Monosphere® 800 beads) are shown. As is already mentioned in the introduction, two systematic errors affect the measurements with this type of nephelometer. First, the 4π integration is limited to scattering angles between 7 and 170° due to

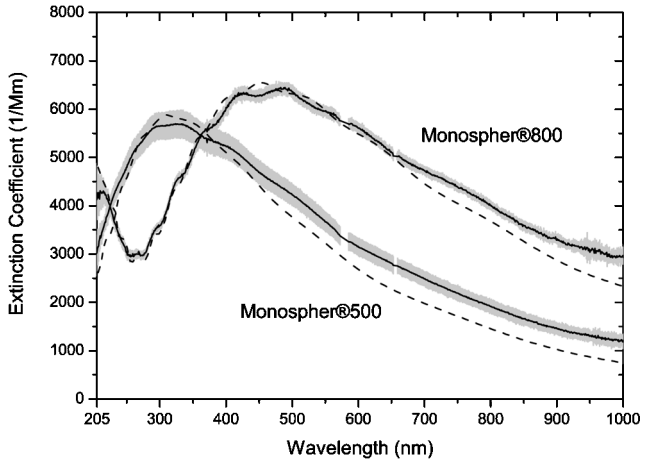

FIG. 4. Comparison of extinction spectra of Monospher® 500 and Monospher® 800 quartz glass beads measured by LOPES (solid lines) and calculated by Mie theory (dashed lines). The shaded area gives the 1-σ standard deviation due to instrument noise and aerosol dilution during 5 min averaging time. Narrow particle size distributions of CMD = 520 nm, σ = 1.05, and CMD = 780 nm, σ = 1.03 are necessary to produce the small scale "ripple structure" clearly visible in the measured spectra. Discrepancies in the exact wavelength position of the ripples and in near-infrared spectral slope are attributed to the presence of small agglomerates.

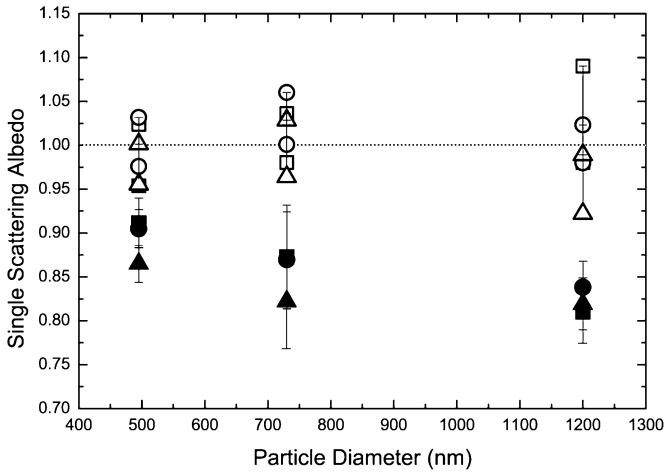

FIG. 5. Experimental verification of the LOPES spectral performance in the visible by comparison of LOPES extinction coefficients with scattering coefficients of a three-color integrating nephelometer at λ = 450 nm (squares), λ = 550 nm (circles), and λ = 700 nm (triangles). Nonabsorbing spherical quartz glass beads (SSA = 1) of different sizes were used as challenge aerosols. Perfect agreement between LOPES and the nephelometer is indicated the by SSA = 1 (open symbols). For reference, we also report the apparent SSA (solid symbols) based on nephelometer values, which are not corrected for angular truncation and non-Lambertian light source.

angular truncation in the forward- and backward-scattering direction. Second, the illumination intensity deviates from the ideal case of a cosine-weighted angular distribution assumed for the standard data evaluation (Anderson et al. 1996; Anderson and Ogren 1998; Heintzenberg and Charlson 1996). These imperfections have been determined experimentally by Anderson et al. 1996 for the TSI 3563 nephelometer. Based on their data we have calculated the nephelometer correction factors accounting for errors due to angular truncation and the non-cosine light source. This was accomplished by first calculating the mean scattering phase function of the particle ensemble and then integrating over 4π solid angle utilizing the ideal and real angular characteristics of the TSI 3563 nephelometer.

Conservative upper and lower limits of the correction factors were estimated based on the geometric standard deviations of the lognormal fit parameters. These yielded upper and lower estimates of the single-scattering albedos, the paired open symbols in Figure 5, which scatter around unity, as expected. The scatter corresponds to an estimated uncertainty of about ± 0.05 in the nephelometer correction factor for submicron-sized aerosol particles in the visible spectral range. This is due to uncertainties in the measured size distribution and the lognormal assumption. Further systematic errors might occur due to nephelometer calibration drifts. Relative 1-σ standard deviations of the K2 calibration constants, describing the correlation of the detected light signal and the scattering coefficient, of 1, 3, and 4% for the 450 n, 550 n, and 700 nm channels, respectively, were deduced from repeated CO_2/air calibrations over the course of the measurement period. Thus, within these uncertainties the extinction and corrected scattering coefficients agree for nonabsorbing spherical aerosol, i.e., in this case Mie theory is applicable to correct for systematic errors in the nephelometer data.

For the Monospher® 500 and Monopher® 800 beads we determined scattering Ångström exponents over the 400 to 700 nm wavelength range, $\alpha_{sca}(450/700)$, with the following relation:

$$\alpha_{sca}\,(450/700) = -\frac{\log\left(b_{sca}^{450}/b_{sca}^{700}\right)}{\log\,(450/700)}. \qquad [8]$$

In case of the Monospher® 500 sample Ångström exponents of 1.46 ± 0.02, 1.46 ± 0.02, and 1.83 were deduced for the measured extinction and scattering coefficients, and for the Mie-calculated extinction (scattering) coefficient, respectively. For the Monospher® 800 beads, significantly lower exponents of 0.67 ± 0.03, 0.67 ± 0.01, and 0.77 were deduced consistent with predictions from Mie theory. Excellent agreement of the Ångström exponents deduced from the LOPES and (corrected) nephelometer measurements emphasize the good spectral performance of LOPES in the visible and indicates that the presented nephelometer correction scheme works for spherical aerosol. However, systematically lower exponents are deduced from the measurements compared to Mie theory, which is likely a result of particle agglomeration as mentioned above.

Soot Aerosol

To derive wavelength-dependent absorption coefficients, b_{abs}^{DM}, from the LOPES data we operate LOPES either in series or parallel with a three-color TSI 3563 nephelometer. Then b_{abs}^{DM} is determined from the difference between extinction and scattering coefficient, Equation (4). Henceforth we will refer to this method as *difference method* (DM).

Applying the laws of error propagation to Equation (4) we find that the relative uncertainty in b_{abs}^{DM} due to the combined nephelometer errors (Δb_{sca}) is less severe for small SSA:

$$\frac{\Delta b_{abs}^{DM}}{b_{abs}^{DM}} = \frac{1}{1-\mathrm{SSA}}\sqrt{\left(\frac{\Delta b_{ext}}{b_{ext}}\right)^2 + \left(\frac{\Delta b_{sca}}{b_{sca}}\mathrm{SSA}\right)^2}. \qquad [9]$$

In fact, for the highly absorbing soot particles used here (SSA $\approx$ 0.2 at 550 nm; Schnaiter et al. 2003), the nephelometer correction is negligible and the overall measurement error is determined by the uncertainty in the LOPES signal, which is dominated by instrument noise (here $\sim$40 Mm^{-1}).

Soot aerosol was either generated by a PALAS model GFG 1000 generator, which produces fractal-like agglomerates by a spark discharge between two graphite electrodes, or extracted from the cleaned exhaust of a VW turbo diesel engine. See Schnaiter et al. (2003) for a detailed discussion of the optical and microphysical properties of both soot types. Experiments with PALAS soot were conducted at the combustion laboratory of the Max Planck Institute for Chemistry in Mainz, Germany (Lobert et al. 1991; Schmid et al. 2004) as well as at the aerosol chamber facility AIDA of Forschungszentrum Karlsruhe, Germany (Kamm et al. 1999). Diesel soot experiments were performed solely at the AIDA facility.

Utilizing Equation (4), b_{abs}^{DM} can be determined at the three nephelometer wavelengths (450, 550, and 700 nm). In order to yield b_{abs}^{DM} at the wavelength of the PAS (532 nm) and MAAP (670 nm), the 450, 550, and 700 nm values of b_{abs}^{DM} are first fitted to

$$\log b_{abs}(\lambda) \sim -\alpha_{abs}\log\lambda \qquad [10]$$

where the fit parameter α_{abs} is the Ångström exponent of absorption. Then b_{abs}^{DM} is determined at $\lambda_2 = 532$ nm (670 nm) by interpolation,

$$\log b_{abs}^{DM}(\lambda_2) = \alpha_{abs}\log\frac{\lambda_2}{\lambda_1} + \log b_{abs}^{DM}(\lambda_1), \qquad [11]$$

where $\lambda_1 = 550$ nm (700 nm).

As shown in Figures 6 and 7, for highly absorbing soot aerosol the absorption coefficients determined by the DM are in excellent agreement with the coefficients measured by PAS

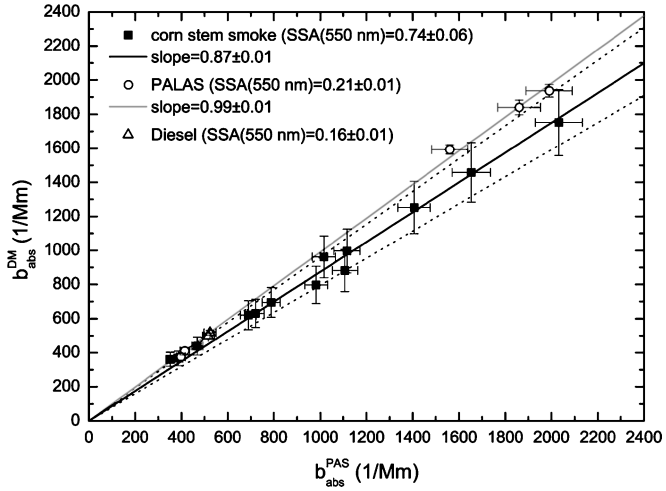

FIG. 6. Comparison between absorption coefficients from the DM and the PAS. Dotted lines: upper and lower limits of $b_{\mathrm{abs}}^{\mathrm{DM}}$ due to uncertainties in the nephelometer correction (for smoke aerosol).

and MAAP, i.e., the regression slopes of 0.99 ± 0.01 and 1.01 ± 0.05 in Figures 6 and 7, respectively, are well within the measurement uncertainties.

We deduced absorption Ångström exponents α_{abs} of 2.2 ± 0.1 and 1.3 ± 0.1 for the PALAS and Diesel soot, respectively. These exponents are in good agreement with values of 2.1 and 1.1 deduced utilizing the difference method in the case of PALAS and Diesel soot during the AIDA Soot Aerosol Campaign in 1999 (Schnaiter et al. 2003).

Biomass Burning Aerosol

As a second example for the DM we investigated the absorption properties of biomass smoke particles that were also generated at the combustion laboratory of the Max Planck Institute for Chemistry in Mainz, Germany. A schematic of the

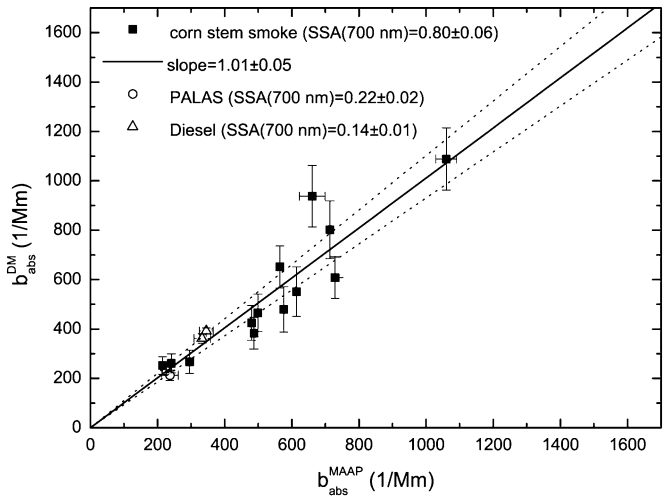

FIG. 7. Same as Figure 6, but for the MAAP instead of the PAS.

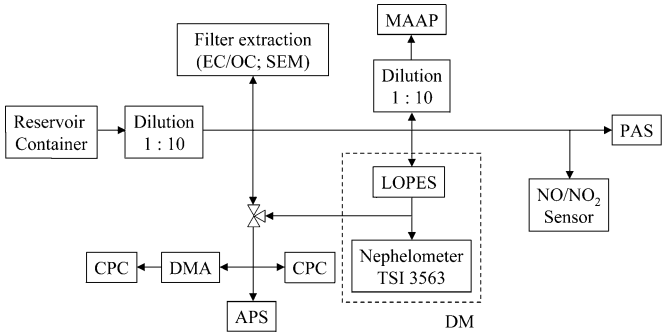

FIG. 8. Experimental setup for the corn stems burning experiments.

experimental setup is depicted in Figure 8. Two separate experiments with corn stems as fuel were performed with a good reproducibility of the experimental data. In both cases the fire emissions were drawn into a well-stirred 32.6 m^3 metal container, which served as a large-volume reservoir for several hours of continuous sampling. To avoid instrument saturation the sample air was diluted by a factor of 10 using a PALAS dilution stage (PALAS, model VKL-10). An additional dilution stage of the same type was used to provide an overall dilution factor of 100 for the MAAP only. The relative humidity downstream of the first Palas dilution stage was kept below 10% to minimize potential systematic effects due to aerosol hygroscopicity. Total aerosol number concentration N was determined with a TSI 3022 CPC, and particle size distributions were measured at selected times with a combination of a TSI 3321 APS and a differential mobility particle sizer (DMPS) consisting of a TSI 3071 DMA (20 nm $< D_p <$ 860 nm) and another TSI 3022 CPC. In addition, filter samples were collected for off-line analysis of particle shape by scanning electron microscopy (SEM) and bulk elemental carbon/organic carbon (EC/OC) content by thermographic analysis according to the German VDI-guideline 2465, part 2 (VDI 1999). We used a thermal carbon analyzer system developed at the Institute of Environmental Technology of the Technical University of Berlin (Ulrich et al. 1990). The analyzer consists of a gas flow control unit for He and O_2 supply, a sample port, a temperature-programmed infraredoven, a CuO/CeO_2 oxidation catalyst for conversion of desorbed hydrocarbons to CO_2, and a ND-IR CO_2 detector. Aerosol samples were deposited on quartz fiber filters (Munktell, type MK 360) which have been prefired at 650°C for at least 12 h prior to sampling. The filter samples were analyzed without any pretreatment by the following three-stage temperature protocol of 8 min duration (Ulrich et al. 1990). First, OC compounds of the aerosol sample were volatilized in a 350°C helium flow (purity grade 5.0). The detected carbon fraction was classified as OC I. Subsequently, low volatile OCs were pyrolyzed in a 650°C helium flow to deduce the OC II fraction. In the last stage the remaining sample was burned in a 650°C oxygen flow (purity grade 4.8) to get the EC fraction. Before switching from helium to oxygen in stage three, the sample was

cooled down to a temperature of 300°C. A high heating rate of 12°C/s was used to avoid charring of hydrocarbons during stage two.

For our experiments, the container was filled with relatively high concentrations of smoke aerosol from the combustion of corn stems (N ~2×10^6 cm^{-3}, b_{sca} (550 nm) ~30,000 Mm^{-1}, b_{abs} (550 nm) ~12,000 Mm^{-1}). After an initial phase dominated by coagulation (~0.5 h) all extensive aerosol parameters (here N, b_{ext}, b_{abs}, and b_{sca}) decreased in the reservoir container at a moderate rate of about 1% per minute mainly due to some coagulation and continuous dilution with relatively clean ambient air (b_{abs} <10 Mm^{-1}, b_{sca} <80 Mm^{-1}). The intercomparison measurements were performed during the latter phase in order to avoid potential biases due to instrument response times. During this period of about 2.5 h the CMD of the number size distribution increased from about 230 to 350 nm and σ_g decreased from about 1.39 to 1.28.

The thermographic analyses yielded EC and OC (= OC I + OC II) fractions of the total carbon mass of about 37 ± 4% and 64 ± 6%, respectively. This rather high EC fraction points to a significant black carbon component of the biomass burning aerosol, which is consistent with the relatively low single scattering albedo (~0.74 at 550 nm). As seen from Figure 9, morphological SEM analysis revealed compact particles of irregular shape.

Figure 10 shows the time evolution of the LOPES extinction spectrum of biomass burning aerosol from corn stems measured at various times after filling the container (here between 0.5 and 2.5 h). With progressing experiment time the extinction spectrum broadens, its maximum gradually shifts toward longer wavelengths, and its amplitude decreases. These findings are consistent with continuous sample dilution (decreasing amplitude) and particle growth due to coagulation (broadening and shift towards longer wavelengths).

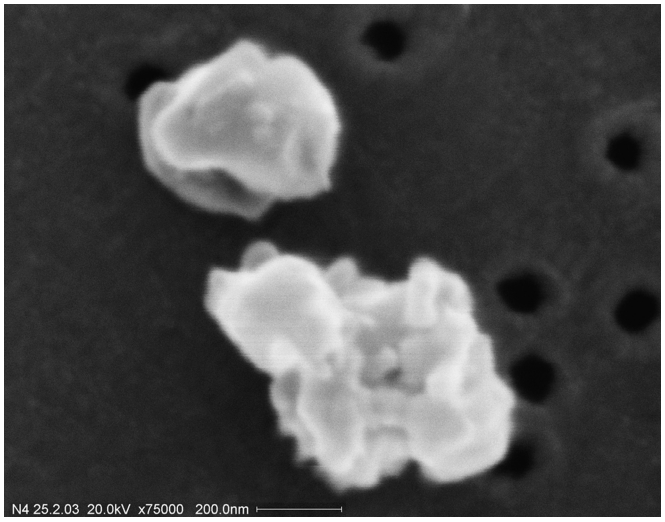

FIG. 9. SEM image of smoke particles from corn stems smoke.

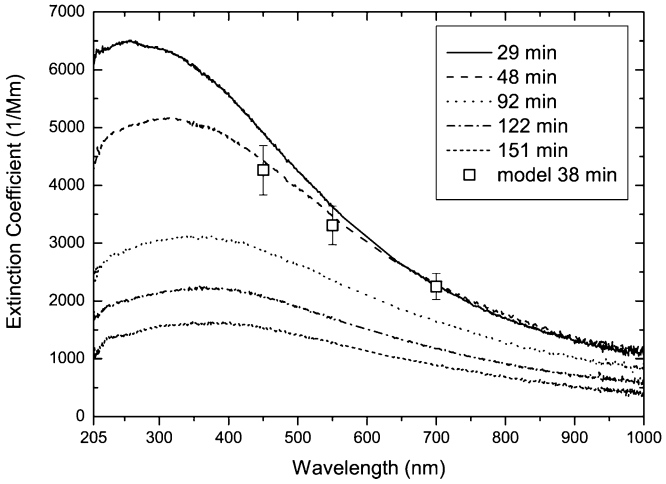

FIG. 10. Time series of extinction spectra measured with LOPES. The squares represent the result of a Mie calculation based on the measured DMPS size distribution and CNC number concentration. A wavelength-dependent refractive index of m (450 nm) = 1.5 + 0.09i, m (550 nm) = 1.5 + 0.07i, and m (700 nm) = 1.5 + 0.05i was assumed.

In contrast to the soot experiments discussed above, the nephelometer correction for angular truncation and noncosine light source is essential to obtain accurate b_{abs}^{DM} values for the biomass burning aerosol. Hence, we first calculated the index of refraction m(450 nm) = 1.5 + 0.09i, m(550 nm) = 1.5 + 0.07i, and m(700 nm) = 1.5 + 0.05i of the biomass burning aerosol by matching the observed SSA (0.69, 0.74, and 0.77) and extinction spectrum to the respective values based on Mie calculation (open squares in Figure 10). This calculation used a lognormal fit (CMD = 270 nm and σ = 1.39) to the DMPS size distribution measured between 34 and 42 min experiment time and the associated CPC particle number concentration (25800 cm^{-3}). With the calculated phase functions we deduced nephelometer correction factors of 1.09, 1.06, and 1.04 for 450, 550, and 700 nm, respectively. In these combined correction factors the error due to the noncosine light source is dominating and has a relative contribution of more than 70%, which is typical for submicron-sized particles (Anderson and Ogren 1998). The decreasing correction factor with increasing wavelength is mainly a result of reduced scattering in the forward direction with decreasing size parameter ($x = \pi D_p/\lambda$). The nephelometer correction factors are found to vary only slightly (e.g., 2-σ deviation of 0.02 at 450 nm) for the size distributions measured over the first 2.5 h experiment time. This might be due to two counteracting effects, the coagulation-induced growth and narrowing of the size distribution. Thus, upper (lower) bounds of 1.11 (1.07), 1.08 (1.04), and 1.05 (1.03) were deduced for the correction factors at 450, 550, and 700 nm, respectively. We note that additional systematic errors in the nephelometer correction may result from uncertainties in refractive index and particle shape (assumed to be spherical). By variation of the real part of the refractive index between 1.5 and 1.7 we estimate the uncertainty

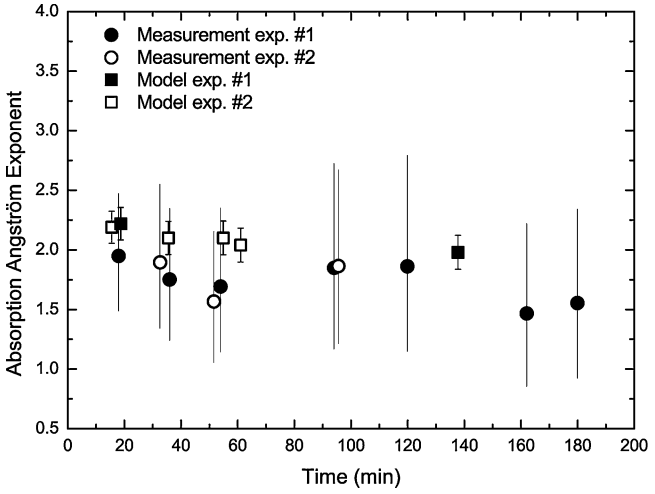

FIG. 11. Time series of the Ångström exponent deduced from b_{abs}^{DM} (circles) and from the modelled absorption cross sections (squares). The error bars of the circles correspond to possible steepest and flattest slopes of b_{abs}^{DM} estimated from the highest and lowest value of b_{abs}^{DM} (according to the 1-σ standard deviation) at $\lambda = 450$ nm and $\lambda = 700$ nm.

due to the former as about 0.02, 0.01, and 0.01 for the correction factors at 450, 550, and 700 nm, respectively. The effect of particle shape on the nephelometer correction factor was not investigated due to the complex nature of the observed particle shape (Figure 9). Thus, combined upper (lower) bounds of 1.13 (1.05), 1.09 (1.03), and 1.06 (1.02) result for the nephelometer correction factors at 450, 550, and 700 nm, respectively.

Figure 11 shows a representative time series of the Ångström exponent of absorption α_{abs} (see Equation [10]) over the course of two experiments. Over 3 h, experiment time α_{abs} decreased moderately from about 1.9 to 1.5 (circles) for an increase in CMD from about 100 to 400 nm. Within the uncertainty of the measurement this size-dependent trend is in agreement with Mie calculations (squares). It is noteworthy that for small particles and weakly absorbing particles, the Rayleigh and Rayleigh-Gans approximations predicts $\alpha_{abs} = 1.0$ under the assumption of a wavelength-independent index of refraction (Bohren and Huffman 1983). Since we have determined a wavelength-dependent imaginary part of the refractive index, our observations are not in disagreement with the Rayleigh and Rayleigh-Gans approximations, and one can conclude that in the small particle limit and in case of weakly absorbing particles enhanced α_{abs} (>1) is consistent with a wavelength-dependent refractive index.

Finally, we return to Figures 6 and 7, which compare the absorption coefficients of the DM with the PAS and MAAP. Please note that while the biomass burning aerosol values in both figures are based on the same data sets, b_{abs}^{MAAP} (670 nm) values are significantly smaller than the corresponding b_{abs}^{PAS} values at 532 nm, which is due to $\alpha_{abs} > 0$ (Equation (10)). Similar to soot particles, there is excellent linear correlation for smoke aerosol over the entire parameter range between about 200 and 2000 Mm^{-1}. However, while for the MAAP the observed slope of 1.01 ± 0.05 is consistent with the soot data and close to the 1:1 line, the PAS slope of 0.87 ± 0.01 indicates that the DM absorption coefficient is 13% lower than the PAS value. Since this is an apparent contradiction to the excellent agreement between DM and PAS for soot particles (slope $= 0.99 \pm 0.01$), it is instructive to consider the measurement errors. The error bars for b_{abs}^{DM} represent the combined uncertainty due to nephelometer calibration drifts as well as the noise of LOPES extinction measurements. The upper and lower bounds attributed to the uncertainties in the nephelometer correction (for biomass burning aerosol) are indicated by the dotted lines in Figures 6 and 7. Hence, the large discrepancy between DM and PAS for smoke aerosol (13%) is a result of b_{abs}^{DM} becoming an increasingly small difference of two large numbers for increasing SSA, which in the limit of SSA $= 1$ leads to a diverging relative uncertainty in b_{abs}^{DM}. In conclusion, we find that the combined experimental uncertainties of b_{abs}^{DM} account for the observed differences to PAS and MAAP for both soot and biomass burning aerosol.

The fact that the measurement error in b_{abs}^{DM} increases with SSA (mainly due to uncertainties in determining the nephelometer correction factors) has important implications for the application of the DM to atmospheric aerosol. Since the SSA of atmospheric aerosol is typically close to about 0.9, the accuracy of b_{abs}^{DM} is expected to be poor. In addition, the relatively low atmospheric extinction coefficients of typically below 100 Mm^{-1} may at least cause significant statistical uncertainty or complete failure due to the LOPES detection limit of $\sim$20 Mm^{-1}. Hence, except for measurements in highly polluted atmospheric regions, LOPES is more suited for laboratory studies.

CONCLUSIONS

The Long Path Extinction Spectrometer (LOPES) is able to measure extinction spectra of laboratory aerosols from $\sim$200 nm to 1015 nm with 2.5 nm spectral resolution and a lower detection limit of 20 Mm^{-1} using an optical path length of 10 m. For glass beads, LOPES showed excellent agreement with the extinction spectrum predicted by Mie theory over the entire spectral range. In addition, LOPES has been combined with a TSI 3563 nephelometer (corrected for truncation and non-Lambertian illumination errors) to determine light absorption by soot and biomass burning aerosols from the difference of extinction and scattering. For both types of aerosol, this DM agreed with the PAS and MAAP, two state-of-the-art absorption techniques operated at a wavelength of 532 and 670 nm, respectively. Hence, LOPES can be used to determine wavelength-resolved optical properties of aerosols, which are needed to calculate the impact of aerosols on short-wave radiative transport through the atmosphere.

Analysis of the propagation of the systematic errors of the TSI 3563 nephelometer into the determination of the absorption coefficient by DM has shown that for aerosols with

single-scattering albedos up to about 0.7 (at 550 nm) the LOPES/TSI 3563 device combination yields wavelength-dependent absorption coefficients with a reasonable accuracy of about 20–25% (combined statistical and systematic errors). For aerosols with higher single-scattering albedos, the DM becomes more uncertain due to subtraction of two large numbers (b_{ext} and b_{sca}). Hence, in this case it is more advisable to combine LOPES with an accurate absorption technique (e.g., MAAP, PAS) to derive $b_{sca} = b_{ext} - b_{abs}$. Since especially for supermicron particles (e.g., dust particles) the systematic errors of integrating nephelometers due to truncation and non-Lambertian light source complicate the direct measurement of b_{sca}, the combination of LOPES with multiwavelength versions of the PAS or MAAP would enhance our capabilities of measuring the optical properties of aerosols. However, limitations due to sensitivity problems of LOPES (>20 Mm^{-1}) have to be acknowledged, restricting its applicability to either laboratory aerosol or to atmospheric environments with sufficiently high aerosol concentrations, as are present in biomass burning smoke plumes or dust storms. An alternative route is to improve integrating nephelometers in a way to reduce both the integration and illumination nonidealities. The prototype single-wavelength nephelometer by Varma et al. (2003) is already a significant step towards the technical realization of this approach.

REFERENCES

Anderson, T. L., and Ogren, J. A. (1998). Determining Aerosol Radiative Properties Using the TSI 3563 Integrating Nephelometer, *Aerosol Sci. Technol.* 29:57–69.

Anderson, T. L., Covert, D. S., Marshall, S. F., Laucks, M. L., Charlson, R. J., Waggoner, A. P., Ogren, J. A., Caldow, R., Holm, R. L., Quant, F. R., Sem, G. J., Wiedensohler, A., Ahlquist, N. A., and Bates, T. S. (1996). Performance Characteristics of a High-sensitivity, Three-wavelength, Total Scatter/Backscatter Nephelometer, *J. Atmos. Oceanic Technol.* 13:967–986.

Arnott, W. P., Moosmüller, H., and Walker, J. W. (2000). Nitrogen Dioxide and Kerosene-flame Soot Calibration of Photoacoustic Instruments for Measurement of Light Absorption by Aerosols, *Rev. Sci. Inst.* 71:4545–4552.

Arnott, W. P., Moosmüller, H., Rogers, C. F., Jin, T. F., and Bruch, R. (1999). Photoacoustic Spectrometer for Measuring Light Absorption by Aerosol: Instrument Description, *Atmos. Environ.* 33:2845–2852.

Bohren, C. F., and Huffman, D. R. (1983). *Absorption and Scattering of Light by Small Particles*. Wiley, New York.

Bond, T. C., Anderson, T. L., and Campbell, D. (1999). Calibration and Intercomparison of Filter-based Measurements of Visible Light Absorption by Aerosols, *Aerosol Sci. Technol.* 30:582–600.

Chylek, P., and Wong, J. (1995). Effect of Absorbing Aerosols on Global Radiation Budget, *Geophys. Res. Lett.* 22:929–931.

Eck, T. F., Holben, B. N., Ward, D. E., Mukelabai, M. M., Dubovik, O., Smirnov, A., Schafer, J. S., Ilsu, N. C., Piketh, S. J., Queface, A., Le Roux, J., and Swap, R. J. (2003). Variability of Biomass Burning Aerosol Optical Characteristics in Southern Africa during the SAFARI (2000) Dry Season Campaign and a Comparison of Single Scattering Albedo Estimates from Radiometric Measurements, *J. Geophys. Res.-Atmos.* 108.

Heintzenberg, J., and Charlson, R. J. (1996). Design and Applications of the Integrating Nephelometer: A Review, *J. Atmos. Oceanic Technol.* 13:987–1000.

Houghton, J. T., Ding, Y., Griggs, D. J., Noguer, M., van der Linden, P. J., and Xiaosu, D. (Eds.). (2001). Climate Change (2001): The Scientific Basis, in *Intergovernmental Panel on Climate Change (IPCC)*, Cambridge University Press, UK.

Huebner, M., Meyer, H., Klein, K.-F., Hillrichs, G., Ruetting, M., Veidemanis, M., Spangenberg, B., Clarkin, J., and Nelson, G. (2000). *Biomedical Optics Symposium (2000)*. Vol. 3911, SPIE-Proc., San Jose, CA, pp. 303312.

Kamm, S., Möhler, O. H., Saathoff, H., and Schurath, U. (1999). The Heterogeneous Reaction of Ozone with Soot Aerosol, *Atmos. Environ.* 33:4651–4661.

Kaufman, Y. J., Hobbs, P. V., Kirchhoff, V. W. J. H., Artaxo, P., Remer, L. A., Holben, B. N., King, M. D., Ward, D. E., Prins, E. M., Longo, K. M., Mattos, L. F., Nobre, C. A., Spinhirne, J. D., Ji, Q., Thompson, A. M., Gleason, J. F., Christopher, S. A., and Tsay, S. C. (1998). Smoke, Clouds, and Radiation—Brazil (SCAR-B) Experiment, *J. Geophys. Res.-Atmos.* 103:31783–31808.

Klein, K. F., Schliessmann, P., Smolka, E., Hillrichs, G., Belz, M., Boyle, W. J. O., and Grattan, K. T. V. (1997). UV-stabilized Silica-based Fibre for Applications around 200 nm Wavelength, *Sensors Actuators B-Chem.* 39:305–309.

Kley, D., and McFarland, M. (1980). Chemiluminescence Detector for NO and NO2, *Atmos. Technol.* 12:63–69.

Lobert, J. M., Scharffe, D. H., Hao, W.-M., Kuhlbusch, T. A., Seuwen, R., Warneck, P., and Crutzen, P. J. (Eds.). (1991). Experimental Evaluation of Biomass Burning Emissions: Nitrogen and Carbon Containing Compounds, in *Global Biomass Burning*, The MIT Press, Cambridge, MA 133–142.

Mishchenko, M. I., Mackowski, D. W., and Travis, L. D. (1995). Scattering of Light by Bispheres with Touching and Separated Components, *Appl. Opt.* 34:4589–4599.

Moosmüller, H. P. (2003). Angular Truncation Errors in Integrating Nephelometry, *Rev. Sci. Inst.* 74:3492–3501.

Palik, E. D. (1985). *Handbook of optical constants of solids*. Academic Press, Orlando, FL.

Petzold, A., and Schönlinner, M. (2004). Multi-angle Absorption Photometry—A New Method for the Measurement of aAerosol Light Absorption and Atmospheric Black Carbon, *J. Aerosol Sci.* 35:421–441.

Petzold, A., Kramer, H., and Schönlinner, M. (2002). Continuous Measurement of Atmospheric Black Carbon Using a Multi-angle Absorption Photometer, *Environ. Sci. Poll. Res.* Special Issue 4:78–82.

Petzold, A., Schloesser, H., Sheridan, P. J., and Arnott, W. P. (2005)). Evaluation of Multi-angle Absorption Photometry for Measuring Aerosol Light Absorption, *Aerosol Sci. Technol.* 39:40–51.

Petzold, A., Fiebig, M., Flentje, H., Keil, A., Leiterer, U., Schroder, F., Stifter, A., Wendisch, M., and Wendling, P. (2002). Vertical Variability of Aerosol Properties Observed at a Continental Site during the Lindenberg Aerosol Characterization Experiment (LACE 98), *J. Geophys. Res.-Atmos.* doi 10.1029/2001JD001043107.

Ramanathan, V., Crutzen, P. J., Lelieveld, J., Mitra, A. P., Althausen, D., Anderson, J., Andreae, M. O., Cantrell, W., Cass, G. R., Chung, C. E., Clarke, A. D., Coakley, J. A., Collins, W. D., Conant, W. C., Dulac, F., Heintzenberg, J., Heymsfield, A. J., Holben, B., Howell, S., Hudson, J., Jayaraman, A., Kiehl, J. T., Krishnamurti, T. N., Lubin, D., McFarquhar, G., Novakov, T., Ogren, J. A., Podgorny, I. A., Prather, K., Priestley, K., Prospero, J. M., Quinn, P. K., Rajeev, K., Rasch, P., Rupert, S., Sadourny, R., Satheesh, S. K., Shaw, G. E., Sheridan, P., and Valero, F. P. J. (2001). Indian Ocean Experiment: An Integrated Analysis of the Climate Forcing and Effects of the Great Indo-Asian Haze, *J. Geophys. Res.-Atmos.* 106:28371–28398.

Reid, J. S., Hobbs, P. V., Liousse, C., Martins, J. V., Weiss, R. E., and Eck, T. F. (1998). Comparisons of Techniques for Measuring Shortwave Absorption and Black Carbon Content of Aerosols from Biomass Burning in Brazil, *J. Geophys. Res.-Atmos.* 103:32031–32040.

Rosencwaig, A. (1980). *Photoacoustics and photoacoustic spectroscopy*. Wiley, New York.

Russell, P. B., Livingston, J. M., Hignett, P., Kinne, S., Wong, J., Chien, A., Bergstrom, R., Durkee, P., and Hobbs, P. V. (1999). Aerosol-induced Radiative Flux Changes off the United States Mid-Atlantic Coast: Comparison of Values Calculated from Sunphotometer and in situ Data with Those Measured by Airborne Pyranometer, *J. Geophys. Res.-Atmos.* 104:2289–2307.

Schnaiter, M., and Wurm, G. (2002). Experiments on Light Scattering and Extinction by Small, Micrometer-sized Aggregates of Spheres, *Appl. Opt.* 41:1175–1180.

Schnaiter, M., Horvath, H., Möhler, O., Naumann, K. H., and Saathoff, H. W. (2003). UV-VIS-NIR Spectral Optical Properties of Soot and Soot-containing Aerosols, *J. Aerosol Sci.* 34:1421–1444.

Sheridan, P. J., Arnott, W. P., Ogren, J. A., Andrews, E., Atkinson, D. B., Covert, D. S., Moosmüller, H., Petzold, A., Schmid, B., Strawa, A. W., Varma, R., and Virkkula, A. (2005). The Reno Aerosol Optics Study: Overview and Summary of Results, *Aerosol Sci. Technol.* 39:1–16.

Terhune, R. W., and Anderson, J. E. (1977). Spectrophone Measurements of the Absorption of Visible Light by Aerosols in the Atmosphere, *Opt. Lett.* 1:70–72.

Ulrich, E., Beckmann, C., and Israel, G. (1990). The Characterization of Carbon Species in Particulate Matter by Successive Thermal-Desorption, *J. Aerosol Sci.* 21:S609–S612.

Varma, R., Moosmüller, H., and Arnott, W. P. (2003). Toward an Ideal Integrating Nephelometer, *Opt. Lett.* 28:1007–1009.

VDI. (1999). Measurement of Soot (Ambient Air)—Thermographical Determination of Elemental Carbon after Thermal Desorption of Organic Carbon, VDI 2465/2 in *VDI/DIN Manual Air Pollution Prevention Volume 4: Analysis and Measurement Methods*, Beuth, W. Berlin, Germany.

Weingartner, E., Saathoff, H., Schnaiter, M., Streit, N., Bitnar, B., and Baltensperger, U. (2003). Absorption of Light by Soot Particles: Determination of the Absorption Coefficient by Means of Aethalometers, *J. Aerosol Sci.* 34:1445–1463.